Eur. Phys. J. A **9**, 479–489 (2000)

THE EUROPEAN PHYSICAL JOURNAL A

The ^{27}Al(p, γ)^{28}Si reaction: direct capture cross-section and resonance strengths at E_p = 0.2–1.12 MeV

S. Harissopulos[1,a], C. Chronidou[1], K. Spyrou[1], T. Paradellis[1], C. Rolfs[2], W.H. Schulte[2], and H.W. Becker[2]

[1] Institute of Nuclear Physics, NCSR "Demokritos", POB 60228, GR-15310 Aghia Paraskevi, Athens, Greece
[2] Institut für Physik mit Ionenstrahlen, Ruhr-Universität-Bochum, Universitätsstrasse 150, D-44780 Bochum, Germany

Received: 4 October 2000 / Revised version: 5 December 2000
Communicated by D. Schwalm

Abstract. The ^{27}Al(p,γ)^{28}Si reaction has been investigated using two different 4π NaI summing detectors. The strength of 26 resonances in the energy range from 200 to 1120 keV has been measured. In addition, yield measurements have been carried out at 9 beam energies in the 490 to 1150 keV range in order to determine the direct capture cross-section. The existing data on the non-resonant mechanism were analysed and combined with the results of the present work. The resulting resonance strengths as well as the deduced direct capture astrophysical S-factor are compared with previous work.

PACS. 25.40.Lw Radiative capture – 25.40.Ny Resonance reactions – 29.40.Mc Scintillation detectors – 27.30.+t $20 \leq A \leq 38$

1 Introduction

The ^{27}Al(p,γ)^{28}Si reaction has been the subject of numerous experimental studies, where resonances have been investigated to beam energies as low as 200 keV [1–3]. The resonances are used for energy and/or efficiency calibration of experimental devices such as accelerators or γ-detectors (*e.g.*, [4]). In addition, the ^{27}Al(p,γ)^{28}Si reaction plays a significant role in nuclear astrophysics [5]: in the hydrogen-burning MgAl cycle it leads to a leakage of nuclei out of the cycle. Due to this role, the ^{27}Al(p,γ)^{28}Si reaction has been included in the compilation of charged-particle–induced thermonuclear reaction rates published by the NACRE collaboration [6]. According to this work, many uncertainties and/or discrepancies between the numerous experimental investigations concerning the resonance strengths $\omega\gamma$ remain to be clarified. These discrepancies may be attributed to systematic errors associated with different setups used as well as with inappropriate normalizations between different measurements. These facts have motivated the present work which completes our recent resonance strength measurements carried out in the energy range E_p = 0.8–2.0 MeV [7]. In the work reported here, several resonances in the E_p = 0.2–1.12 MeV range have been investigated under identical experimental conditions, *e.g.*, using the same detector, target and backing material. In addition, direct capture cross-section measurements have been carried out since the existing data on this are poor [8,9].

In the present work, the γ-spectra have been obtained using 4π NaI(Tl) summing crystals. The main advantage hereby is that, instead of measuring and analysing numerous γ-cascade transitions, the response of the NaI(Tl) crystals leads predominantly to a single peak, called the sum peak, at the sum of the energies of the cascading transitions. As a result, a prominent peak arises in the measured γ-spectra at an energy $E_\gamma = Q + E_{\rm cm}$, where Q is the Q-value of the reaction and $E_{\rm cm}$ is the center-of-mass energy. Due to the 4π geometry covered by the summing crystals, the observed γ-ray fluxes are angle integrated; thus, systematic errors due to γ-angular distribution effects are eliminated.

2 Experimental setups and procedures

2.1 Resonance strength measurements

All measurements reported in this subsection have been carried out at the Dynamitron Tandem Laboratorium (DTL) of the Ruhr-Universität Bochum. Proton beams have been provided by the 450 kV single-stage accelerator (SAMES) as well as by the 4 MV tandem accelerator. The beam energy spread of SAMES was about 0.2 keV, whereas that of the tandem was less than 1 keV at E_p = 1 MeV. The current of the SAMES beam on target varied in the 4–40 μA range, whereas that of the tandem was kept in the 0.5–2 μA range in order to minimize dead time effects (below 2%).

The experimental setup has been described elsewhere [10,11]. The main component is a 12 inch × 12 inch NaI(Tl)

[a] e-mail: sharisop@mail.demokritos.gr

summing crystal with a central bore hole of 35 mm diameter and a 0.5 mm Al wall thickness. The crystal could be moved on a rolling tray so that the target could be placed in the center of the crystal.

Targets have been produced by evaporating different amounts of Al on 0.5 mm thick Cu backings. Before the evaporation procedure all Cu backings were etched, polished, and cleaned with soap. In addition, a 10 μg/cm^2 thick Al target on a 0.5 mm thick Ta foil has been used. All targets were frequently checked for deterioration, stability, and carbon-buildup on their surface by carrying out appropriate yield checks and rescans of certain resonances as well as via off beam optical controls. In addition, when starting a run with a new target, the yield on the "plateau" of at least two resonances already scanned in the former runs was checked.

The Cu backed targets were appropriate to obtain thick target yields. Two targets, for which 30 μg/cm^2 Al was evaporated on the Cu backing, were found to have a thickness of about 10±1 keV at the $E_{\rm R}$ = 406 keV resonance. Three other Cu-backed targets, for which 50 μg/cm^2 Al was evaporated on the backing, had a thickness of 15±1 keV and 10±1 keV at the $E_{\rm R}$ = 406 keV and $E_{\rm R}$ = 1025 keV resonances, respectively. These targets have been used to measure the strength of the resonances in the 0.4–1.12 MeV range, whereas the former two targets have been used to investigate resonances in the 0.20–0.45 MeV region. The Ta-backed target was found to have a thickness of about 3.5±0.5 keV at $E_{\rm R}$ = 760 keV, sufficiently thin to resolve resonances in the 720–800 keV and 1080–1140 keV region and to obtain the respective thick target yields.

2.2 Direct capture cross-section measurements

Cross-section measurements in the non-resonant energy region have been carried out at the DTL as well as at the tandem laboratory of the Institute of Nuclear Physics of NCSR Demokritos, Athens. Gamma-spectra have been obtained at proton energies, which were selected according to a minimum contribution of resonance tails: E_p = 490, 570, 600, 722, 820, 850, and 980 keV (at Bochum) and E_p = 850, 980, 1070, and 1155 keV (at Athens). The setup at Bochum was described above and that at Athens elsewhere [7,12]. The data points taken at E_p = 850 and 980 keV in both sets of measurements served to check the compatibility of the results.

In the measurements at Bochum, the beam current was in the 2.2–5.0 μA range and the total charge collected on the target varied from 8 to 15 mCb. The thickness of the Al targets (on Cu backings) has been determined using the narrow resonances at $E_{\rm R}$ = 446, 632, and 887 keV leading to 53.3±1.6 and 43.2±2.2 μg/cm^2. The thicker target has been used to carry out cross-section measurements at E_p = 490, 570 and 600 keV, while the thinner one has been used at E_p = 722, 820, 850, and 980 keV. Both targets were frequently checked for deterioration by scanning the narrow resonances at $E_{\rm R}$ = 446, 632, and 887 keV and were found to be stable within 2%. In addition to the above experiments, yield measurements of the Cu-backings have been performed at the same beam energies in order to determine and subtract the yield arising from the ^{63,65}Cu(p,γ)^{64,66}Zn reactions induced by the protons in the Cu-backings. It was found that the yield due to these contaminant reactions was between 5% and 20% of the total yield measured at E_p = 490, 570, and 600 keV, whereas at E_p = 722, 822, 850, and 980 keV it was negligible.

In the second set of measurements (Athens), the cross-section has been measured with one single target at E_p = 850, 980, 1070, and 1155 keV. The Al target (on Cu backing) had a thickness of 47.3±2.4 μg/cm^2 as determined using the $E_{\rm R}$ = 992 keV resonance. The same resonance has been used to calibrate the accelerator as well as to check for possible target deterioration; the target was stable within 0.5%. The beam current was about 1.2 μA and the charge collected on the target was about 4.2 mCb. The energy spread of the proton beam was found to be 1.6 keV at E_p = 1 MeV. Yield measurements of the Cu-backing have also been carried out without changing any beam focusing parameter, *i.e.* at the end of each run the target was rotated by 180° and γ-spectra of the Cu-backing have been taken for an equal charge. Hence, the *net* reaction yield could be determined. A sample spectrum at E_p = 980 keV resulting from the subtraction of the backing background from the total yield spectrum is presented in fig. 1. Hereby, the sum peak can be seen at an energy $E_\gamma = E_{\rm cm} + Q = 0.945 + 11.584 = 12.529$ MeV.

3 Data analysis and results

3.1 The ^{27}Al+p resonances

In order to determine the resonance strengths $\omega\gamma$, the following procedure has been carried out. Firstly, each resonance was scanned by varying the proton energy. Each γ-spectrum taken was corrected for dead time effects, accumulated charge, and cosmic-ray contributions. The number of counts in the sum peak (fig. 2) was then used

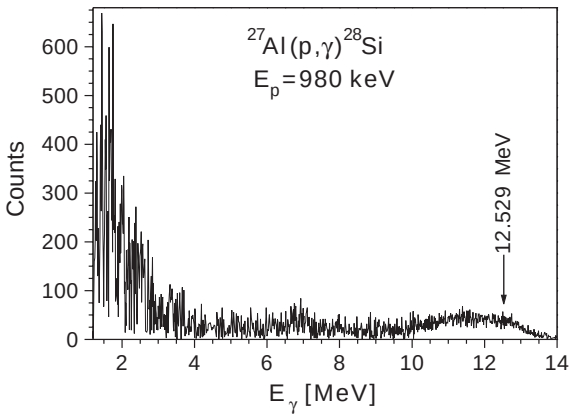

Fig. 1. Gamma spectrum obtained at E_p = 980 keV after subtracting the background due to the Cu-backing.

to obtain a resonance yield curve including a sharp low-energy edge, a plateau, and a high-energy edge (fig. 3). After obtaining this yield curve, spectra with high statistics were obtained at a beam energy on the plateau (= ON-spectrum) and at a beam energy slightly lower than the low-energy edge of the yield curve (= OFF-spectrum). The subtraction of the OFF-spectrum from the ON-spectrum resulted in a difference spectrum from which total yields were derived for every resonance. This procedure is illustrated in fig. 2 for the case of the E_R = 992 keV resonance. The spectrum shown in part a) of fig. 2 is the

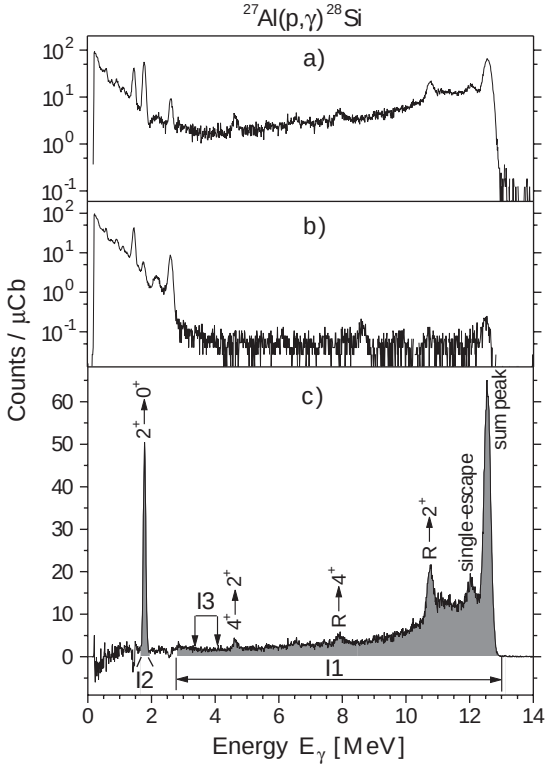

Fig. 2. Gamma spectra taken a) at the plateau of the E_R = 992 keV resonance and b) at E_p = 988 keV, just below the resonance. The spectrum in c) is the difference of spectra a) and b). The peaks due to the γ-transitions from the resonant state to the 4^+ and 2^+ level are indicated as R$\rightarrow 4^+$ and R$\rightarrow 2^+$, respectively. One can also see the secondary transitions $4^+ \rightarrow 2^+$ and $2^+ \rightarrow 0^+$, the single-escape peak, as well as the sum peak.

ON-spectrum, whereas that shown in part b) is the corresponding OFF-spectrum taken at a beam energy of 988 keV; the difference spectrum is shown in part c). Normally, the whole integral of the difference spectrum corresponds to the total yield of the resonance under study. However, as can be seen in the difference spectrum of fig. 2, the energy region below E_γ = 2.8 MeV is not always smooth (non-shaded region). As this might lead to uncertainties in the integrations, the number of counts of the difference spectra have been obtained using the sum of three integration regions as shown in fig. 2. The shaded region "I1" includes all events with energies $E_\gamma \geq 2.8$ MeV. The shaded region "I2" is the peak arising from the $2^+ \rightarrow 0^+$ secondary γ-transition. In the third region "I3" the number of counts is rather constant. Thus, region "I3" serves to obtain the remaining yield, *i.e.* the yield of the non-shaded region of the spectrum; this is done by multiplying the integral of region "I3" with the width ratio of the non-shaded region to region "I3". The latter procedure was recommended by the work of Mehrhoff [13]. From the resulting thick target yield Y_∞, the corresponding resonance strength $\omega\gamma$ was calculated using the formula

$$Y_\infty = \frac{N_A}{A}\varepsilon\frac{\lambda^2}{2}\omega\gamma\frac{M+m}{M}\frac{1}{T(E)}\,, \qquad (1)$$

where $T(E)$ is the stopping power of the target, ε is the detection efficiency, N_A is the Avogadro number, and A is the atomic weight of the target. The stopping power values $T(E)$ were obtained from [14], and the detection efficiency has been adopted from [13], *i.e.* $\varepsilon = 91 \pm 9\%$. This efficiency has been found to be independent of the number of cascade transitions and energy of the photons [13,15]. This value is in good agreement with the result of Monte Carlo calculations carried out via GEANT [16]. The resulting thick target yields and resonance strengths are summarized in table 1.

3.2 Non-resonant mechanism

The direct capture astrophysical S-factor $S_{DC}(E)$ has been determined by means of the following procedure:

1. From the net reaction yield the *total* cross-section $\sigma_T(E)$ has been determined.
2. Using $\sigma_T(E)$, the *total* astrophysical S-factor $S_T(E)$ has been derived.
3. From the known properties of the ^{27}Al+p resonances in the 400–1300 keV range, an S-factor $S_R(E)$ attributed only to the resonant mechanism has been calculated.
4. The S-factor due to the non-resonant process $S_{DC}(E)$ has been deduced from $S_{DC}(E) = S_T(E) - S_R(E)$.

In the case of the spectra taken in Bochum, the window of integration used to obtain the net reaction yield has been set to the sum peak, in order to exclude γ-rays arising from reactions of the beam with target impurities, *i.e.* mainly the ^{19}F(p, $\alpha\gamma$)^{16}O reaction. The absolute efficiency ε of the Bochum NaI summing crystal has been determined by Mehrhoff [13] via Monte Carlo simulations using GEANT. For the particular window of integration used in the present measurements, Mehrhoff [13] has found $\varepsilon = 21 \pm 4\%$.

The absolute efficiency of the NaI summing detector used in Athens has been determined also via Monte Carlo simulations and the results of the respective calculations have been confirmed experimentally by measuring well-known resonances of three nuclear reactions as described in [12]. The window of integration used to derive the net

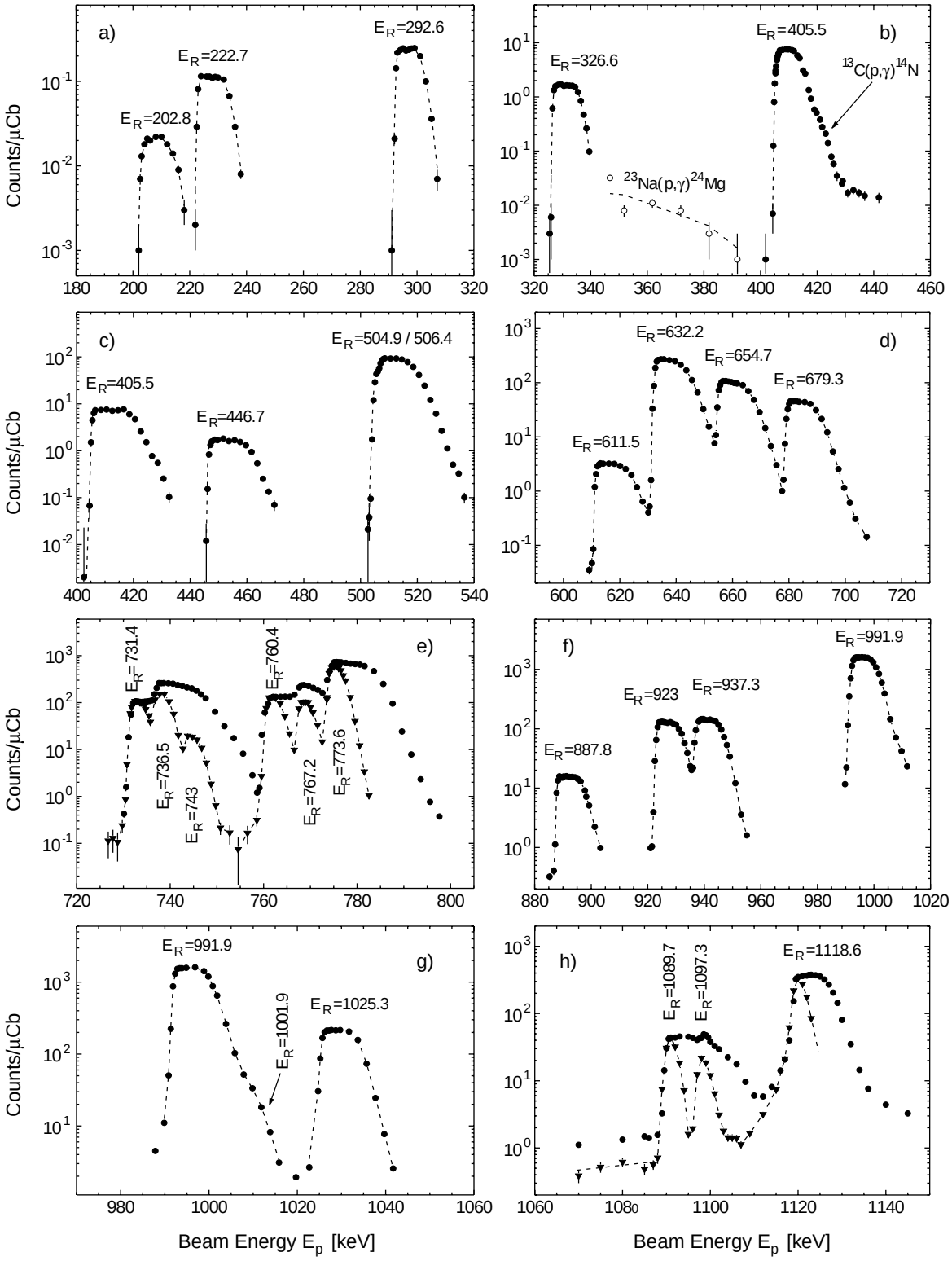

Fig. 3. Yield curves of resonances at $E_{\mathrm{R}} = 0.2$ to 1.2 MeV. The dotted lines are to guide the eye only. Curves shown in a) and b) have been measured via the 30 μg/cm^2 thick targets. The yield curves shown with solid triangles in e) and h) have been determined using the 10 μg/cm^2 thick Ta-backed target. The other yield curves have been measured with different Al-targets which had a thickness of 50 μg/cm^2. The comparison of the plateaus of the latter targets with those of the Ta-backed targets (triangles) shows that from the latter plateaus thick target yields can be obtained for all resonances shown in e) and h).

Table 1. Thick target yields Y_∞ and resonance strengths $\omega\gamma$. The resonance energies $E_{\rm R}$ have been adopted from [3]. The given Y_∞ values are the average result of at least two independent efficiency corrected yields that have been determined using different targets.

$E_{\rm R}$ (keV)	Y_∞ (Counts/μC)	$\omega\gamma$ (eV)
202.8	0.094(13)	$1.10(15)\times10^{-5}$
222.7	0.40(3)	$5.0(4)\times10^{-5}$
292.6	1.9(1)	$2.80(15)\times10^{-4}$
326.6	13.3(7)	$2.10(11)\times10^{-3}$
405.3	58(3)	$1.04(5)\times10^{-2}$
446.7	9.4(7)	$1.80(15)\times10^{-3}$
504.9	151(19)	$3.1(4)\times10^{-2}$
506.4	204(24)	$4.1(5)\times10^{-2}$
611.5	26(3)	$5.8(7)\times10^{-3}$
632.2	1296(130)	0.29(3)
654.7	538(53)	0.12(1)
679.3	249(26)	$5.8(6)\times10^{-2}$
731.4	591(34)	0.142(8)
736.5	726(52)	0.175(15)
743.0	94(10)	$2.30(25)\times10^{-2}$
760.4	556(39)	0.14(1)
767.2	802(57)	0.200(15)
773.6	1696(170)	0.42(4)
887.8	44(5)	$1.20(15)\times10^{-2}$
923.0	551(55)	0.145(15)
937.3	721(72)	0.19(2)
991.9	7308(517)	2.00(15)
1025.3	1318(132)	0.36(4)
1089.7	303(22)	$8.4(6)\times10^{-2}$
1097.3	150(16)	$4.2(4)\times10^{-2}$
1118.6	2978(298)	0.85(9)

reaction yield from the γ-spectra was from 8 to 15 MeV. For this particular window the absolute efficiency has been calculated considering mainly γ_0 and γ_1 decays of ^{28}Si and has been found to be $52 \pm 3\%$.

The total reaction cross-section $\sigma_{\rm T}(E)$ has been derived from the net reaction yield mentioned above by using, as described in [5], the relation

$$Y(E_p) = \int_{E_p-\Delta(E_p)}^{E_p} \frac{\sigma_{\rm T}(E)}{T(E)}{\rm d}E\,, \qquad (2)$$

where $Y(E_p)$ is the net reaction yield observed at an incident beam energy E_p, $T(E)$ is the stopping power and $\Delta(E_p)$ the target thickness at E_p in energy units. The stopping power $T(E)$ is in most cases nearly constant over the energy interval $E_p - \Delta(E_p)$. Hence, $T(E)$ can be removed from the above integral, *i.e.*

$$Y(E_p) = \frac{1}{T(E)} \int_{E_p-\Delta(E_p)}^{E_p} \sigma_{\rm T}(E){\rm d}E. \qquad (3)$$

If the cross-section is a slowly varying function of energy, *i.e.* it is constant over the interval $E_p - \Delta(E_p)$, then the effective energy in the target is

$$E_{\rm eff} = E_p - \frac{\Delta(E_p)}{2} \qquad (4)$$

and the cross-section at this energy is given by

$$\sigma_{\rm T}(E_{\rm eff}) = Y(E_p)\frac{T(E_p)}{\Delta(E_p)}. \qquad (5)$$

In our case $E_{\rm eff}$ corresponds to the beam energy in the target, at which one-half of the yield for the full target thickness is obtained. In the present work, all reaction cross-sections have been obtained by applying the latter relation. From the total reaction cross-sections obtained by using eq. (5), the respective astrophysical S-factors have been calculated using the expression:

$$S(E_{\rm cm}) = \sigma_{\rm T}(E_{\rm cm})E_{\rm cm}e^{2\pi\eta} \qquad (6)$$

where η is the Sommerfeld parameter. In our case, eq. (6) can be rewritten as

$$S(E_{\rm cm}) = \sigma_{\rm T}(E_{\rm cm})E_{\rm cm}e^{400.939/\sqrt{E_{\rm cm}}}. \qquad (7)$$

where $\sigma_{\rm T}(E_{\rm cm})$ is given in barn, $E_{\rm cm}$ in keV, and $S(E_{\rm cm})$ in keV $\cdot$ barn.

Equation (7) has also been used to derive the S-factor due to a single narrow isolated resonance. The total cross-section $\sigma_{\rm T}(E)$ has been replaced by the cross-section $\sigma_{\rm R}(E)$ due to the resonance in consideration. The quantity $\sigma_{\rm R}(E)$ was calculated according to the Breit-Wigner formula

$$\sigma_{\rm R}(E) = \sigma_{\rm R}(E_{\rm R})\frac{E_{\rm R}}{E}\frac{\Gamma_a(E)}{\Gamma_a(E_{\rm R})}\frac{\Gamma_b(E)}{\Gamma_b(E_{\rm R})} \times\frac{(\Gamma(E_{\rm R})/2)^2}{(E-E_{\rm R})^2+(\Gamma(E)/2)^2}, \qquad (8)$$

where Γ_a and Γ_b are the partial widths of the entrance and exit channels, respectively, and Γ is the total width, *i.e.* $\Gamma = \Gamma_a + \Gamma_b$. In our case,

$$\frac{\Gamma_a(E)}{\Gamma_a(E_{\rm R})} = \left(\frac{E_{\rm R}}{E}\right)^{1/2}\frac{P_l(E)}{P_l(E_{\rm R})}\,, \qquad (9)$$

where P_l are the penetration factors that have been obtained numerically, and

$$\frac{\Gamma_b(E)}{\Gamma_b(E_{\rm R})} = \left(\frac{E_\gamma}{E_{\gamma,E=E_{\rm R}}}\right)^3, \qquad (10)$$

where $E_\gamma = E_{\rm cm}+Q$. The cross-section $\sigma_{\rm R}(E_{\rm R})$ of a given resonance was calculated via the expression:

$$\omega\gamma = \sigma_{\rm R}(E_{\rm R})\Gamma_{\rm R}\frac{\pi}{\lambda^2}. \qquad (11)$$

The total widths $\Gamma_{\rm R} := \Gamma(E = E_{\rm R})$ used in the latter equation have been taken from [3]. Hereby, as for some resonances only upper limits are reported in [3], these

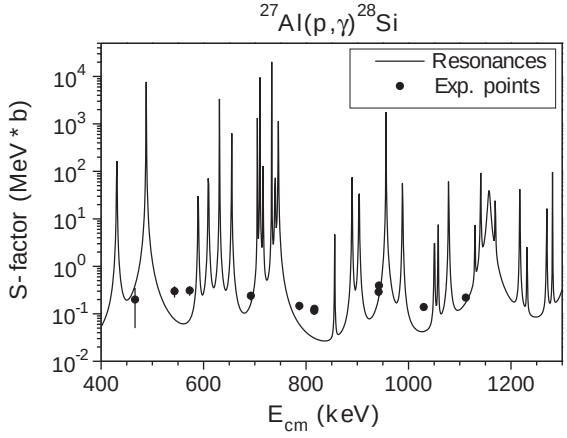

Fig. 4. Experimentally deduced S-factor (solid points) and S-factor due to all resonances present at $E_{\rm cm} = 400$–1300 keV (solid curve).

limits have been adopted as the values of $\Gamma_{\rm R}$. The resonance strengths $\omega\gamma$ used, are the corresponding averages of the NACRE compilation [6] and the results of the present work. The S-factors deduced for each resonance present in the 400–1300 keV range have been added in order to derive the S-factor $S_{\rm R}(E)$ due to the resonant mechanism. This is presented in fig. 4 (solid curve) together with the total S-factors $S_{\rm T}(E)$ determined in the present work at 9 beam energies (solid points). By subtracting the solid curve from the solid points of fig. 4, one obtains the S-factor $S_{\rm DC}$, due to the direct capture mechanism. The resulting values for $S_{\rm DC}$ are listed in table 2. The values given for $E_{\rm cm} = 816$ and 942 keV are the weighted average of the two values shown in fig. 4 that have been measured independently, in Bochum and Athens. The S-factor reported by Lyons *et al.* in [8], which is the only available information on the direct capture process, is also given. Hardie *et al.* [9] have measured γ-angular distributions of the capture to the ground state (γ_0) as well as to the first excited state (γ_1) by using Ge(Li) detectors. By fitting Legendre polynomials to this data set we deduced the nonresonant total cross-sections σ_{γ_0} and σ_{γ_1} of the γ_0 and γ_1 transitions, respectively. Using these cross-section values and applying eq. (7), the nonresonant astrophysical S-factors S_{γ_0} and S_{γ_1} of the γ_0 and γ_1 transitions, respectively, have been derived. Hereby, the effective energies used in eq. (7) have been derived by subtracting 5 keV from the beam energies used by Hardie *et al.* [9], since in the latter work the energy spread caused by the slowing down of the beam in the target was given as ≈10 keV. Furthermore, by assuming that the γ_0 and γ_1 transitions are those that mainly contribute to the direct capture cross-section, the *total* direct capture S-factor $S_{\rm T}$ has been extracted as $S_{\rm T} = S_{\gamma_0} + S_{\gamma_1}$ at $E_{\rm cm} = 783.7$, 814.6, 1017.8, 1094.1, 1559.7, and 1715.9 keV. At these energies, the contribution of the resonance tails to the reaction yield is –according to fig. 4– minimized. The resulting $S_{\rm T}$ values are given in table 3. In order to include as many data points as possible in our subsequent analysis, we deduced $S_{\rm T}$ at the additional energies $E_{\rm cm} = 559.1$, 1007.4, and 1550.1 keV by multiplying the corresponding S_{γ_1} values with the average $\bar{\lambda} = 1.22(4)$ of the ratios $\lambda = S_{\rm T}/S_{\gamma_1}$ given in table 3.

Table 2. Astrophysical S-factor for the ^{27}Al(p,γ)^{28}Si reaction.

$E_{\rm cm}$ (keV)	$S_{\rm DC}$ (keV b) present work	$S_{\rm DC}$ (keV b) ref. [8]
466	≤ 112	
543	220 ± 80	
573	230 ± 70	
692	70 ± 50	
787	87 ± 30	
816	94 ± 12	
942	139 ± 41	
1022		77 ±40
1030	97 ± 17	
1112	70 ± 70	

Table 3. S-factors deduced by analysing the differential cross-section data reported in [9].

$E_{\rm cm}$ (keV)	S_{γ_0} (keV b)	S_{γ_1} (keV b)	$\lambda = S_{\gamma_1} + S_{\gamma_0}/S_{\gamma_1}$	$S_{\rm T}$ (keV b)
525.4		130(26)		
559.1		94(13)		115(16)
689.3		88(11)		
783.7	12(2)	33(9)	1.36(47)	45(9)
814.6	10(2)	46(9)	1.22(31)	56(9)
929.3		119(14)		
1007.4		62(8)		76(10)
1017.8	12(2)	65(8)	1.18(19)	77(8)
1085.5		75(10)		
1094.1	14(2)	82(10)	1.17(19)	96(10)
1108.6		113(14)		
1184.8		158(19)		
1195.4		137(16)		
1206.9		209(25)		
1369.8		363(44)		
1374.7		245(29)		
1389.1		201(24)		
1550.1		61(9)		74(9)
1559.7	13(2)	74(12)	1.18(19)	87(9)
1569.4		95(15)		
1583.8		131(16)		
1588.7		344(41)		
1715.9	20(3)	56(9)	1.36(22)	76(8)
			$\bar{\lambda} = 1.22(4)$	

4 Discussion

4.1 Resonance strengths

As already discussed in the introduction, Endt and coworkers [1–3] have compiled experimental data reported

Table 4. Compilation of resonance strengths for ^{27}Al(p,γ)^{28}Si at $E_p = 0.2$–1.12 MeV.

E_R^{lab} (keV)	Present $\omega\gamma$ (eV)	NACRE [6] $\omega\gamma$ (eV)	Others (the refs. are given in brackets at the end of the coressponding $\omega\gamma$ values) $\omega\gamma$ (eV)
202.8	$1.10(15)\times10^{-5}$	$1.4(7)\times10^{-5}$	$1.4(7)\times10^{-5}$ [22]
222.7	$5.0(4)\times10^{-5}$	$9(2)\times10^{-5}$	$11.4(35)\times10^{-5}$ [21], $7.8(25)\times10^{-5}$ [18]
292.6	$2.80(15)\times10^{-4}$	$3.8(7)\times10^{-4}$	$3.7(11)\times10^{-4}$ [21], $3.5(18)\times10^{-4}$ [18]
326.6	$2.10(11)\times10^{-3}$	$1.5(3)\times10^{-3}$	$1.71(53)\times10^{-3}$ [21], $2.3(5)\times10^{-3}$ [18], $1.92(42)\times10^{-3}$ [8], $0.8(3)\times10^{-4}$ [20]
405.3	$1.04(5)\times10^{-2}$	$0.9(1)\times10^{-2}$	$0.71(22)\times10^{-2}$ [21], $1.25(25)\times10^{-2}$ [18], $1.0(2)\times10^{-2}$ [8], $0.65(28)\times10^{-4}$ [20]
446.7	$1.80(15)\times10^{-3}$	$1.4(2)\times10^{-3}$	$1.43(44)\times10^{-3}$ [21], $1.5(5)\times10^{-3}$ [8], $1.42(61)\times10^{-3}$ [20]
504.9	$3.1(4)\times10^{-2}$	$6.1(7)\times10^{-2}$	$3.7(12)\times10^{-2}$ [17], $4.5(19)\times10^{-2}$ [20]
506.4	$4.1(5)\times10^{-2}$	$4.2(9)\times10^{-2}$	$3.7(12)\times10^{-2}$ [17], $5.5(24)\times10^{-2}$ [20]
611.5	$5.8(7)\times10^{-3}$	$4(1)\times10^{-3}$	$14.3(44)\times10^{-3}$ [21], $4.92(75)\times10^{-3}$ [20]
632.2	0.29(3)	0.266(14)	0.286(88) [21], 0.208(53) [17], 0.442(67) [23], 0.25(3) [8] 0.30(4) [24], 0.26(3) [25], 0.268(13) [26], 0.216(43) [27]
654.7	0.12(1)	0.12(9)	0.114(35) [21], 0.125(33) [17], 0.116(14) [8], 0.125(26) [25], 0.129(56) [20]
679.3	$5.8(6)\times10^{-2}$	$4.5(5)\times10^{-2}$	$4.3(13)\times10^{-2}$ [21], $3.92(125)\times10^{-2}$ [17], $5.4(7)\times10^{-2}$ [8], $6.5(28)\times10^{-2}$ [20]
731.4	0.142(8)	0.12(1)	0.114(35) [21], 0.15(4) [17], 0.129(16) [8], 0.110(47) [20]
736.5	0.175(15)	0.160(16)	0.157(48) [21], 0.167(50) [17], 0.159(21) [8], 0.181(78) [20]
743.0	$2.30(25)\times10^{-2}$	$2.1(3)\times10^{-2}$	$2.86(88)\times10^{-2}$ [21], $1.42(4)\times10^{-2}$ [17], $2.67(58)\times10^{-2}$ [8], $2.6(11)\times10^{-2}$ [20]
760.4	0.14(1)	0.135(16)	0.143(44) [21], 0.133(42) [17], 0.126(17) [8], 0.181(78) [20]
767.2	0.200(15)	0.16(2)	0.171(53) [21], 0.158(50) [17], 0.175(25) [8], 0.135(58) [20]
773.6	0.42(4)	0.41(3)	0.457(141) [21], 0.39(13) [28], 0.458(142) [29], 0.408(50) [8], 0.442(83) [24], 0.613(264) [20], 0.383(77) [27]
887.8	$1.20(15)\times10^{-2}$	$1.5(2)\times10^{-2}$	$2.00(66)\times10^{-2}$ [21], $1.33(25)\times10^{-2}$ [8], $2.00(86)\times10^{-2}$ [20], $1.20(10)\times10^{-2}$ [7]
923.0	0.145(15)	0.140(18)	0.171(53) [21], 0.130(17) [8], 0.213(92) [20], 0.140(13) [7]
937.3	0.19(2)	0.176(21)	0.171(53) [21], 0.175(53) [30], 0.175(25) [8], 0.194(10) [20], 0.183(17) [7]
991.9	2.00(15)	1.9(1)	3.17(50) [31], 1.83(20) [8], 1.88(23) [25], 1.93(13) [26], 2.00(17) [32], 1.94(7) [7]
1025.3	0.36(4)	0.31(3)	0.314(97) [21], 0.325(42) [8], 0.245(106) [20], 0.342(68) [27], 0.35(3) [7]
1089.7	0.084(6)	0.08(1)	0.071(22) [21], 0.090(11) [8], 0.065(28) [20], 0.080(23) [27]
1097.3	0.042(4)	0.04(1)	0.034(11) [21], 0.045(5) [8], 0.029(13) [20], 0.043(12) [7]
1118.6	0.85(9)	0.73(13)	0.60(18) [21], 1.208(125) [33], 0.85(9) [8], 1.208(125) [34], 0.708(75) [35], 0.574(247) [20], 0.80(6) [7]

on the ^{27}Al+p resonances. The resonance strengths measured in the present work are compared in table 4 with the $\omega\gamma$-values reported in the literature. In this comparison, the compilations of Endt *et al.* [1–3] have not been taken into account for the following reasons: In [1], the resonance strengths adopted have been initially taken from [17–19]. Hereby, the values from [17] and [19] have been matched to $\omega\gamma = 0.85(25)$ eV at $E_p = 773$ keV. This value, however, is rather ambiguous since it completely disagrees with the results of other experimental data (table 4). Hence, the $\omega\gamma$-values adopted in [1] have been here discarded as they are the results of an ambiguous normalization. This applies also to the values given in [2], since they have been taken from [1]. In the last compilation [3], the author has adopted the results of mainly one experimental work [20]. It has to be noticed that from the references given in table 4, only 5 references [7,8,21,17,20] are systematic investigations of the ^{27}Al+p resonances in the region $E_p \leq 1.15$ MeV. On the other hand, [6] is the most recent relevant compilation. The rest of the references given in table 4 report mainly on a single or very few resonance strength measurements and will therefore not be discussed further.

From table 4, the $\omega\gamma$ values adopted by the NACRE compilation [6] agree satisfactorily with our results: The comparison reveals deviations of at least 20% for the resonances at $E_R = 203$, 223, 293, 327, 447, 505, 612, 679, and 767 keV. However, when using the 2σ criterion, discrepencies remain only at $E_R = 223$, 505 and 612 keV. The comparison of the $\omega\gamma$-values measured in the present work, with the respective results of Chronidou *et al.* [7] reveals an excellent agreement. Good agreement is also found with the data of Lyons *et al.* [8]. In the work of Broström *et al.* [21] the strength of the $E_R = 992$ keV resonance is 7 eV, considerably higher than the value from previous and present work; furthermore, no errors are quoted. Hence, we have normalized all $\omega\gamma$-values of [21] to our result for the $E_R = 992$ keV resonance and estimated a 30% error. The resulting values, which are also given in table 4, are in relatively good agreement with our data. The $\omega\gamma$-values reported in [17] have been deduced using as reference value $\omega\gamma = 0.39(13)$ eV at $E_R = 773$ keV from [28]. Our result for the latter resonance is 0.42(4) eV, and is well within the uncertainties of the value of [28]. The resonance strengths of [17] are in satisfactory agreement with our results when taking into account the 2σ-criterion. Finally, the $\omega\gamma$-values reported by Meyer *et al.* [20] have been deduced by normalizing their data to $\omega\gamma = 0.44$ eV at $E_R = 632$ keV. This value, adopted by the authors from [23], deviates from all reported values (table 4) and

Table 5. Total reaction rates $\langle\sigma v\rangle$ derived in the present work for different stellar temperatures T. The lower and upper limits of the $\langle\sigma v\rangle$ values are indicated as $\langle\sigma v\rangle_{\rm low}$ and $\langle\sigma v\rangle_{\rm high}$ respectively.

T 10^9 (K)	$\langle\sigma v\rangle$	$\langle\sigma v\rangle_{\rm low}$ ($\rm mole^{-1}$ $\rm cm^3$ $\rm s^{-1}$)	$\langle\sigma v\rangle_{\rm high}$	T 10^9 (K)	$\langle\sigma v\rangle$	$\langle\sigma v\rangle_{\rm low}$ ($\rm mole^{-1}$ $\rm cm^3$ $\rm s^{-1}$)	$\langle\sigma v\rangle_{\rm high}$
0.010	4.47×10^{-37}	3.60×10^{-37}	5.33×10^{-37}	0.16	4.25×10^{-5}	3.81×10^{-5}	4.69×10^{-5}
0.011	1.23×10^{-35}	9.90×10^{-36}	1.47×10^{-35}	0.18	1.95×10^{-4}	1.75×10^{-4}	2.15×10^{-4}
0.012	2.30×10^{-34}	1.86×10^{-34}	2.75×10^{-34}	0.20	6.70×10^{-4}	6.06×10^{-4}	7.35×10^{-4}
0.013	3.17×10^{-33}	2.56×10^{-33}	3.81×10^{-33}	0.25	6.80×10^{-3}	6.22×10^{-3}	7.37×10^{-3}
0.014	3.39×10^{-32}	2.72×10^{-32}	4.22×10^{-32}	0.30	3.66×10^{-2}	3.39×10^{-2}	3.94×10^{-2}
0.015	2.99×10^{-31}	2.33×10^{-31}	4.37×10^{-31}	0.35	1.37×10^{-1}	1.27×10^{-1}	1.47×10^{-1}
0.016	2.33×10^{-30}	1.66×10^{-30}	5.15×10^{-30}	0.40	4.02×10^{-1}	3.75×10^{-1}	4.29×10^{-1}
0.018	1.41×10^{-28}	5.38×10^{-29}	8.20×10^{-28}	0.50	2.16×10^{-1}	2.00×10^{0}	2.32×10^{0}
0.020	7.84×10^{-27}	1.07×10^{-27}	6.67×10^{-26}	0.60	7.80×10^{0}	7.18×10^{0}	8.43×10^{0}
0.021	4.93×10^{-26}	4.14×10^{-27}	4.48×10^{-25}	0.70	2.16×10^{1}	1.98×10^{1}	2.35×10^{1}
0.022	2.69×10^{-25}	1.47×10^{-26}	2.52×10^{-24}	0.80	4.97×10^{1}	4.53×10^{1}	5.41×10^{1}
0.023	1.28×10^{-24}	4.83×10^{-26}	1.23×10^{-23}	0.90	9.87×10^{1}	8.98×10^{1}	1.08×10^{2}
0.024	5.37×10^{-24}	1.49×10^{-25}	5.21×10^{-23}	1.00	1.75×10^{2}	1.60×10^{2}	1.91×10^{2}
0.025	2.02×10^{-23}	4.30×10^{-25}	1.97×10^{-22}	1.25	5.21×10^{2}	4.76×10^{2}	5.67×10^{2}
0.03	3.96×10^{-21}	4.15×10^{-23}	3.91×10^{-20}	1.50	1.13×10^{3}	1.03×10^{3}	1.22×10^{3}
0.04	2.74×10^{-18}	3.22×10^{-20}	2.70×10^{-17}	1.75	2.00×10^{3}	1.84×10^{3}	2.17×10^{3}
0.05	1.36×10^{-16}	6.49×10^{-18}	1.29×10^{-15}	2.0	3.14×10^{3}	2.88×10^{3}	3.40×10^{3}
0.06	6.86×10^{-15}	4.54×10^{-15}	2.22×10^{-14}	2.5	6.04×10^{3}	5.53×10^{3}	6.55×10^{3}
0.07	9.68×10^{-13}	8.36×10^{-13}	1.18×10^{-12}	3.0	9.51×10^{3}	8.66×10^{3}	1.04×10^{4}
0.08	4.85×10^{-11}	4.24×10^{-11}	5.48×10^{-11}	3.5	1.32×10^{4}	1.20×10^{4}	1.45×10^{4}
0.09	1.02×10^{-9}	9.00×10^{-10}	1.15×10^{-9}	4	1.69×10^{4}	1.52×10^{4}	1.87×10^{4}
0.10	1.17×10^{-8}	1.03×10^{-8}	1.31×10^{-8}	5	2.39×10^{4}	2.11×10^{4}	2.67×10^{4}
0.11	8.59×10^{-8}	7.60×10^{-8}	9.58×10^{-8}	6	2.97×10^{4}	2.58×10^{4}	3.37×10^{4}
0.12	4.50×10^{-7}	4.00×10^{-7}	5.01×10^{-7}	7	3.44×10^{4}	2.94×10^{4}	3.94×10^{4}
0.13	1.83×10^{-6}	1.62×10^{-6}	2.03×10^{-6}	8	3.80×10^{4}	3.21×10^{4}	4.40×10^{4}
0.14	6.05×10^{-6}	5.40×10^{-6}	6.71×10^{-6}	9	4.07×10^{4}	3.39×10^{4}	4.75×10^{4}
0.15	1.70×10^{-5}	1.53×10^{-5}	1.89×10^{-5}	10	4.26×10^{4}	3.50×10^{4}	5.01×10^{4}

is by a factor 1.5 higher than our result. Hence, we renormalized the results of [20] to our $\omega\gamma$-value at $E_{\rm R} = 992$ keV. The resulting resonance strengths are given in table 4. They are statistically in good agreement with our results except for those at $E_{\rm R} = 327$, 405 and 612 keV.

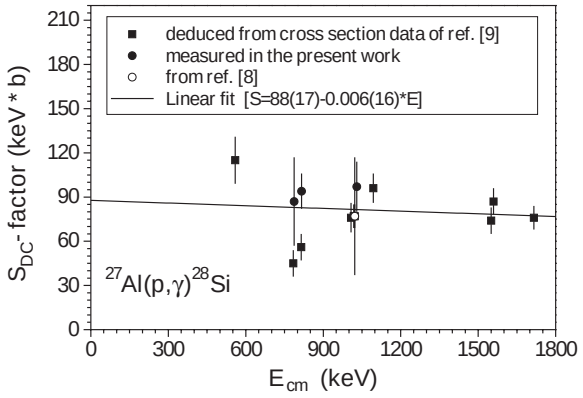

Fig. 5. Direct capture S-factors *vs* center-of-mass energy $E_{\rm cm}$. The solid squares are the results of the analysis of the cross-section data reported in [9]; the solid circles are the results of the present work; the open circle has been obtained from [8].

4.2 S-factors

From fig. 4 one can distinguish which of the data points $S_{\rm T}(E)$ fulfils the criterion of minimum contribution by the resonance tails, *i.e.* the data points at $E_p = 466$, 692, 942 and 1112 keV are not appropriate for further analysis of direct capture data. Consequently, the respective $S_{\rm DC}$-factors of table 2 have to be discarded. From the remaining $S_{\rm DC}$ values the points at $E_p = 543$ and 573 keV exhibit rather large errors. If these data points are taken into account in a linear fit, often used to determine the $S_0 := S_{\rm DC}(E = 0)$ value, one obtains rather uncertain results. A more realistic approximation is to take the S_0-factor via the average value of the $S_{\rm DC}$-factors measured at $E_p = 787$, 816, 1022, and 1030 keV. In this case, one obtains $S_0 = 89 \pm 9\,{\rm keV\ b}$.

The $S_{\rm T}$-factors extracted from the data of [9] (table 3) are shown in fig. 5 together with the S-factors measured in the present work at $E_{\rm cm} = 787$, 816, and 1030 keV. In the same figure the S-factor reported by [8] is also plotted. A linear fit to the data points shown in fig. 5 yields (with E in keV)

$$S(E) = 88(17) - 0.006(16) \cdot E\,[\,{\rm keV\,b}\,]\,. \qquad (12)$$

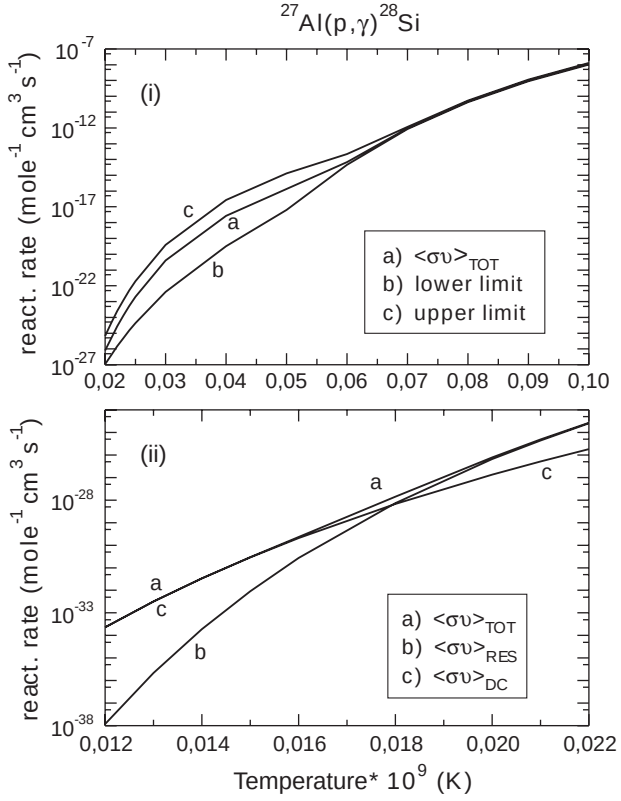

Fig. 6. (i) Total reaction rate $\langle\sigma v\rangle_{\rm T}$ (curve "a") at temperatures $0.02 \cdot 10^9 \leq T \leq 0.1 \cdot 10^9$ K. The corresponding lower and upper limits are given by curves "b" and "c", respectively. (ii) Contribution of the resonant (curve "b") and non-resonant (curve "c") mechanism to the total reaction rate (curve "a") at temperatures $T \leq 0.022 \cdot 10^9$ K.

Both S_0 values, determined either via the linear fitting procedure ($S_0 = 88 \pm 17$ keV b) or as the average value of the $S_{\rm DC}$-factors measured at $E_p = 787$, 816, 1022, and 1030 keV ($S_0 = 89 \pm 9$ keV b) are within the statistical errors close to the value $S_0 = 70$ keV b ($\pm 20\%$) deduced from theoretical calculations [36].

4.3 Reaction rates

The rate $\langle\sigma v\rangle$ of a nuclear reaction is used as input parameter in astrophysical calculations. The ^{27}Al(p,γ)^{28}Si reaction is of key importance when the Mg-Al cycle and/or Silicon burning are considered in the calculations [37]. Hence, the resonance strengths and the S-factors resulting from the present data analysis have been used to derive $\langle\sigma v\rangle$ values, in order to provide a consistent set of reaction rates.

The total rate $\langle\sigma v\rangle_{\rm T}$ of a given reaction is given [5] as the sum

$$\langle\sigma v\rangle_{\rm T} = \langle\sigma v\rangle_{\rm R_b} + \langle\sigma v\rangle_{\rm R_n} + \langle\sigma v\rangle_{\rm R_{DC}} \qquad (13)$$

where $\langle\sigma v\rangle_{\rm R_b}$ and $\langle\sigma v\rangle_{\rm R_n}$ are the rates due to broad and narrow-isolated resonances, respectively, and $\langle\sigma v\rangle_{\rm DC}$ is

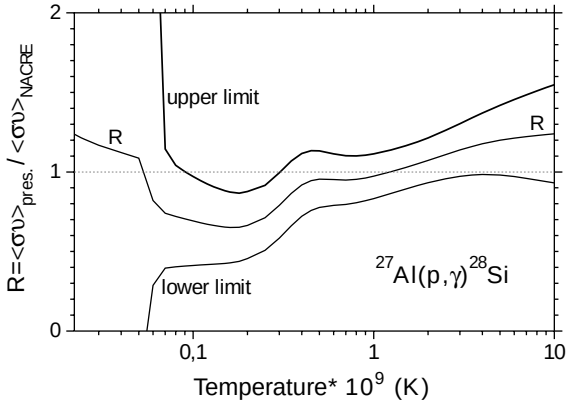

Fig. 7. Ratio of the reaction rate determined in the present work to that given in the NACRE compilation [6].

the rate contribution from the direct capture process (non-resonant part). In the case of ^{27}Al(p,γ)^{28}Si no broad resonances are present. Hence, the total reaction rate can be calculated as the sum of the contributions from the narrow-isolated resonances and the direct capture only. In such a case, the following equation has to used [5]:

$$\langle\sigma v\rangle_{\rm T} = \sqrt{\frac{8}{\pi\mu}}\left(\frac{1}{kT}\right)^{3/2}\int_0^\infty S(E)e^{\left(-\frac{E}{kT}-\frac{b}{E^{1/2}}\right)}{\rm d}E + \left(\frac{2\pi}{\mu kT}\right)^{3/2}\hbar^2\sum_i(\omega\gamma)_i e^{\left(-\frac{E_i}{kT}\right)}. \qquad (14)$$

where μ is the reduced mass, k is the Boltzmann constant, T is the temperature, $S(E)$ is the astrophysical factor, and $(\omega\gamma)_i$ is the resonance strength of the resonance i at E_i center-of-mass energy. The quantity b is given by the equation $b = 0.989 Z_1 Z_2 \mu^{1/2}$, with Z_1 and Z_2 being the atomic numbers of the projectile and the target nucleus, respectively. The first term of the sum in eq. (14) is the contribution of the direct capture, whereas the second one is the reaction rate due to the individual resonances.

In our analysis, we first replaced $S(E)$ in eq. (14), with the analytical expression given by eq. (12), which has been obtained by the fitting procedure discussed in section 4.2. Then we performed the numerical calculation of the integral of eq. (14). Furthermore, in order to calculate the second term of eq. (14), we used the $\omega\gamma$ values determined in the present work as well as those reported by Chronidou *et al.* in [7]. At overlapping energy regions, average values have been adopted for the resonance strengths involved. For resonances at $E_p < 0.19$ MeV and $2.05\,{\rm MeV} < E_p < 3.96$ MeV, we used the $\omega\gamma$ values given in the NACRE compilation [6].

It has to be mentioned that, in addition to the contribution of the narrow resonances to the total reaction rate, one also has to consider contributions of the resonance tails. Hence, for each resonance one has to calculate the following quantity:

$$\langle\sigma v\rangle_{\rm tail} = \sqrt{\frac{2}{\mu}}\frac{\Delta}{kT^{3/2}}S(E_0)\exp\left(-\frac{3E_0}{kT}\right), \qquad (15)$$

where E_0 is the Gamow peak energy and Δ is the width of the Gamow peak [5], which in our case –indicatively– are $E_0 = 65$ keV, $\Delta = 15$ keV at $T = 0.03 \cdot 10^9$ K and $E_0 = 2.21$ MeV, $\Delta = 1.23$ MeV at $T = 6 \cdot 10^9$ K. The quantity $\langle \sigma v \rangle_{\rm tail}$ has been calculated for each resonace. It was however found to be negligibly small in all cases, and therefore it was not taken into account.

The total reaction rates deduced in the present work are listed in table 5. According to these results and as shown in fig. 6(i), the total rate has large errors at temperatures $T \leq 0.065 \cdot 10^9$ K. At this temperature the corresponding Gamow peak is at $E_0 = 105$ keV and the respective Gamow width is $\Delta = 30$ keV. It is known, that below 100 keV there are two known resonances, at $E_{\rm R} = 75$ and 88 keV. These resonances are extremely weak. However, the errors quoted in the NACRE compilation [6] for their strengths are huge. Hence, the large uncertainties in the total reaction rate calculated in the present work can be explained. From the comparison of the deduced reaction rates due to the resonant mechanism with that due to the direct capture process we find that the latter mechanism dominates at low temperatures, $T \leq 0.018 \cdot 10^9$ K. This is shown in fig. 6(ii).

A comparison of the reaction rates deduced in the present work with those given in the NACRE compilation [6] is shown in fig. 7. Hereby the ratio of the present reaction rates over the respective NACRE values is plotted at different temperatures. From fig. 7, we conclude that at $T \leq 0.3 \cdot 10^9$ K, at which the corresponding Gamow peak energy is $E_0 \approx 300$ keV, as well as at $T \geq 5 \cdot 10^9$ K ($E_0 \approx 2$ MeV), the resulting total reaction rates deviate from those given in the NACRE compilation by more than 20%.

5 Conclusions

In the present work, 26 resonances of the ^{27}Al(p,γ)^{28}Si reaction have been investigated from $E_p = 200$ to 1120 keV. The use of a large 4π Na(I) summing crystal enabled us to carry out angle integrated measurements. Hence, any angular distribution effects have been eliminated. By using the same experimental conditions in all runs, we could avoid uncertainties arising from normalizations between measurements in different laboratories. Our results are based on a self-consistent efficiency correction method. Most of the resonance strengths measured in the present work are in good agreement with those adopted in the NACRE compilation [6].

In addition, direct capture cross-section measurements have been carried out. The astrophysical S-factors determined are statistically in agreement with those predicted [36]. Reaction rates have also been deduced in the present work. The resulting large uncertainties at stellar temperatures corresponding to energies $E_p \leq 100$ keV suggest that further low-energy measurements of resonance strengths (*e.g.*, at the underground accelerator laboratory in Gran Sasso = LUNA) are necessary in this energy region.

References

1. P. M. Endt, C. Van der Leun, Nucl. Phys. **34**, 1 (1962).
2. P. M. Endt, C. Van der Leun, Nucl. Phys. A **105**, 1 (1967).
3. P. M. Endt, Nucl. Phys. A **521**, 1 (1990).
4. T. Freye, H. Lorenz-Wirzba, B. Cleff, H. P. Trautvetter, C. Rolfs, Z. Phys. A **281**, 211 (1977).
5. C. Rolfs, W.S. Rodney, Cauldrons in the cosmos (University of Chicago Press, 1988).
6. **N**uclear **A**strophysics **C**ompilation of **RE**action Rates (**NACRE**): C. Angulo, M. Arnould, M. Rayet, P. Descouvemont, D. Baye, C. Leclerq-Willain, A. Coc, S. Barhoumi, P. Auger, C. Rolfs, R. Kunz, J.W. Hammer, A. Mayer, T. Paradellis, S. Kossionides, C. Chronidou, K. Spyrou, S. Degl'Innocenti, G. Fiorentini, B. Ricci, S. Zavaratelli, C. Providencia, H. Walters, J. Soares, C. Crama, J. Rahighi, A. Shotter, M. Lamehi Rachti, Nucl. Phys. A **656**, 3 (1999) and NACRE Web-site: http://pntpm.ulb.ac.be/nacre.htm
7. C. Chronidou, K. Spyrou, S. Harissopulos, S. Kossionides, T. Paradellis, Eur. Phys. J. A **6**, 303 (1999).
8. P.B. Lyons, J.W. Toevs, D.G. Sargood, Nucl. Phys. A **130**, 1 (1969).
9. G. Hardie, R. E. Segel, A. J. Elwyn, J. E. Monahan, Phys. Rev. C **38**, 2003 (1988).
10. D. Zahnow, C. Angulo, C. Rolfs, S. Schmidt, W. H. Schulte, E. Somorjai, Z. Phys. A **351**, 229 (1995).
11. K. Spyrou, C. Chronidou, S. Harissopulos, S. Kossionides, T. Paradellis, C. Rolfs, W.H. Schulte, L. Borucki, Eur. Phys. J. A **7**, 79 (2000).
12. K. Spyrou, C. Chronidou, S. Harissopulos, S. Kossionides, T. Paradellis, Z. Phys. A **357**, 283 (1997).
13. M. Mehrhoff, Diplomarbeit, (Ruhr-Universität-Bochum, Bochum 1996), unpublished.
14. H.H. Andersen and J.F. Ziegler, *Hydrogen Stopping Powers and Ranges in All Elements*, Volume 3, (Pergamon Press, New York 1997).
15. C. Chronidou, Ph. D. Thesis, (National Technical University, Athens 1997), unpublished.
16. *GEANT-Detector description and Simulation Tool*, (CERN, Geneva 1993).
17. P. M. Endt, A. Heyligers, Physica **26**, 230 (1960).
18. K. Okano, J. Phys. Soc. Japan **15**, 28 (1960).
19. R. Nordhagen, Nucl. Inst. Meth. **12**, 291 (1961).
20. M. A. Meyer, I. Venter, D. Reitman, Nucl. Phys. A **250**, 235 (1975).
21. K. J. Brostroem, T. Huus, R. Tangen, Phys. Rev. **71**, 661 (1947).
22. P.J.M. Smulders, P.M. Endt, Physica **28**, 1093 (1962).
23. G. A. P. Engelbertink, P. M. Endt, Nucl. Phys. **88**, 12 (1966).
24. M. M. Aleonard, C. Boursiuot, P. Hubert, P. Mennrath, Phys. Lett. B **49**, 40 (1974).
25. Z. E. Switkowski, R. OBrien, A. K. Smith, D. G. Sargood, Aust. J. Phys. **28**, 141 (1975).
26. B. M. Paine, D. G. Sargood, Nucl. Phys. A **331**, 389 (1979).
27. J. Brenneisen, D. Grathwohl, M. Lickert, R. Ott, H. Röpke, J. Schmälzlin, P. Siedle, B. H. Wildenthal, Z. Phys. A **352**, 149 (1995).
28. P. B. Smith, P. M. Endt, Phys. Rev. **110**, 397 (1958).
29. A. Luuko, Soc. Sci. Fenn. Comm. Phys.-Mat. **31** (1965) Nr. 6.
30. R. Nordhagen, Nucl. Phys. **44**, 130 (1963).

31. E. Spring, Soc. Sci. Fenn. Comm. Phys.-Mat. **28** (1963) Nr. 6.
32. J. Keinonen, S. Brandenburg, Nucl. Phys. A **341**, 345 (1980).
33. R. Nordhagen, A. Tveter, Nucl. Phys. **63**, 529 (1965).
34. J. R. Leslie, W. McLatchie, C. F. Mohanan, J. K. Thrasher, Nucl. Phys. A **170**, 115 (1971).
35. J. Dalmas, F. Leccia, M. M. Aleonard, Phys. Rev. C **9**, 2200 (1974).
36. R. Timmermann, H.W. Becker, C. Rolfs, U. Schröder, H.P. Trautvetter, Nucl. Phys. A **477**, 105 (1988).
37. R. M. Cavallo, A. V. Sweigart, R. A. Bell, Astroph. J. **464**, L79 (1996).